Supplementary Materials

Dictionary Replacement for Single Image Restoration of 3D Scenes

T M Nimisha
ee13d037@ee.iitm.ac.in
M Arun
ee14s002@ee.iitm.ac.in
A N Rajagopalan
raju@ee.iitm.ac.in

Image Processing and Computer Vision Lab
Indian Institute of Technology, Madras
Chennai, India

In this supplementary material, we provide additional results on synthetic and real experiments. The restored images used for the quantitative analysis described in the main paper are also provided. All images are best viewed in pdf.

1 Synthetic experiments

We begin with the synthetic case whose PSNR were given in Fig. 5 of main paper. Here we discuss the qualitative nature of those results. We also provide an additional synthetic result on the Map dataset from Middlebury.

Qualitative results obtained for the defocus case corresponding to the PSNR plot of Fig. 5(a) in the main paper is shown in Fig. A1. The ground truth (GT) latent images corresponding to the dataset used are given in Fig. A1(a). These images are subjected to space-variant Gaussian blur where the blur grids are shown in Fig. A1(b). The resultant space-variantly blurred images are shown in Fig. A1(c). We compared with the methods NCSR [6] and SRDB [28], as discussed in the main paper. The results obtained using these methods along with our results are shown in Figs. A1(d-f). The zoomed-in patches for the respective inputs, outputs and comparison results are also shown below each example. Since NCSR and SRDB perform space-invariant deblurring, they can properly deblur only those regions that lie on a single depth layer. Performance in other regions is poor. This can be clearly seen from the zoomed-in patches provided for two different depth layers in Figs. A1(g) and (h).

Qualitative results corresponding to motion blur (Fig. 5(b) in main paper) are shown in Fig. A2. We use the same latent images provided in Fig. A1(a) and blur using the space-variant motion blur grids shown in Fig. A2(a). Motion blur applied to each input differed in direction and length. The synthesized blurred images are given in Fig. A2(b). Here, we compared with NCSR [6], Hu et al. [9] and Xu et al. [27]. The results obtained using these methods along with our results are shown in Figs. A2(c-f), respectively. The quality of our deblurred result is better than the state-of-the-art methods (see the zoomed-in patches in Fig. A2(g)).

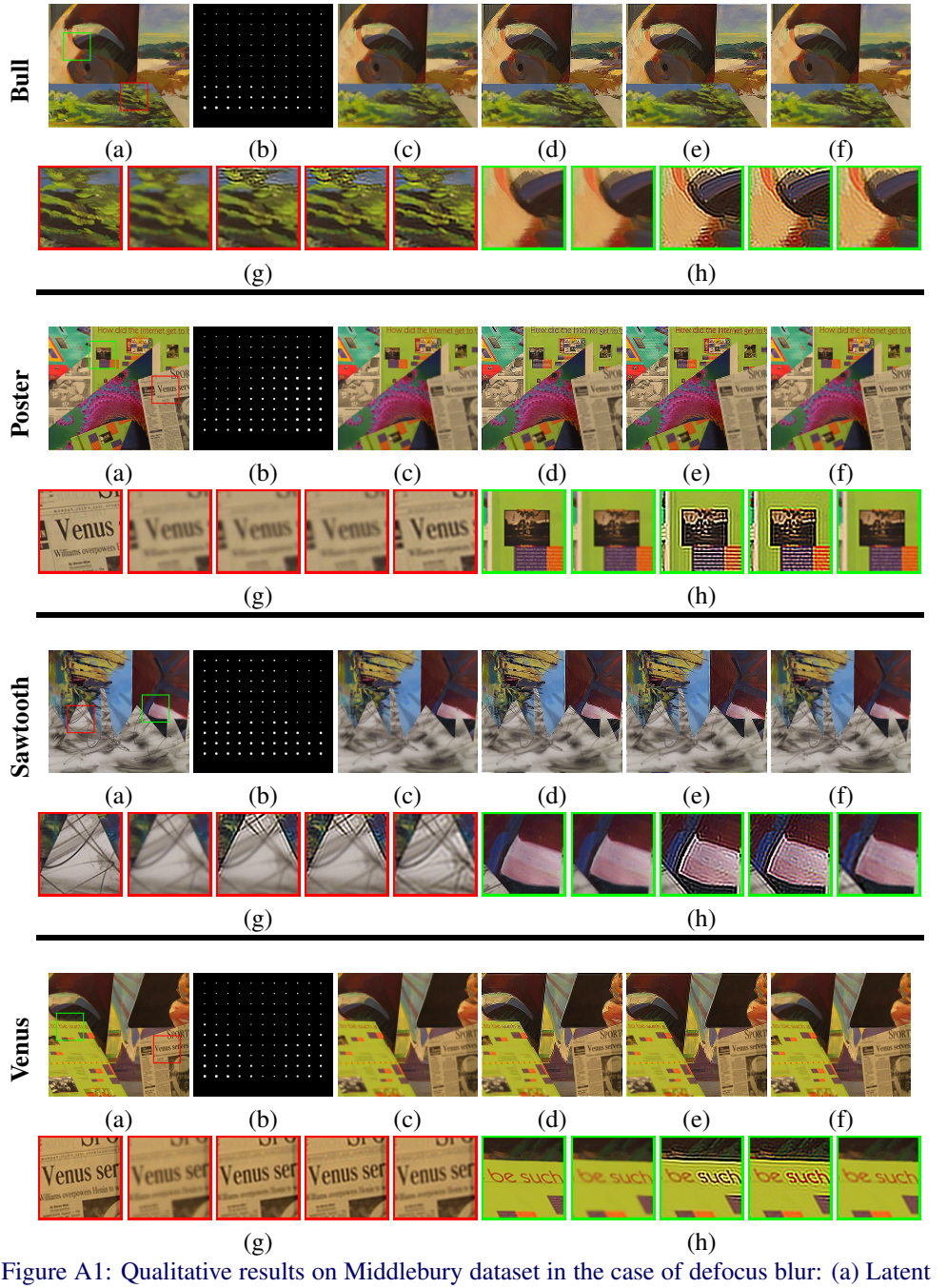

Figure A1: Qualitative results on Middlebury dataset in the case of defocus blur: (a) Latent input image. (b) Defocus kernel grid. (c) Blurred input. (d-f) Deblurred result obtained by NCSR, SRDB and our method, respectively. (g-h) Zoomed-in patches corresponding to two different depth layers extracted from (a) and (c-f) in the same order.

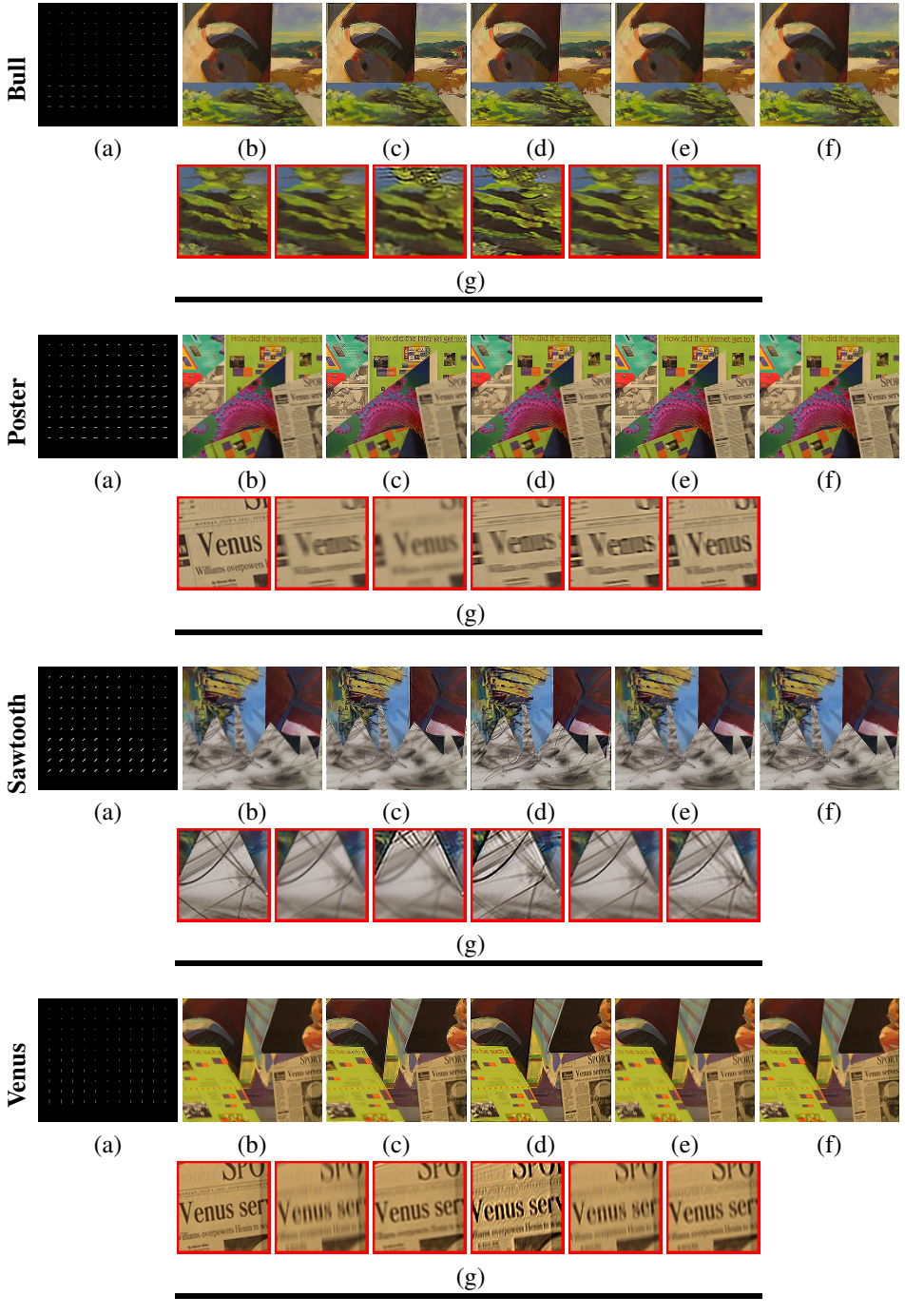

Figure A2: Synthetic Experiment on Middlebury dataset in the case of Motion blur: (a) Kernel grid. (b) Blurred input. (c-f) Deblurring results obtained by NCSR, Hu. et al., Xu et al. and our proposed method, respectively. (g) Zoomed-in patches extracted from the latent image and (b-f) in the same order.

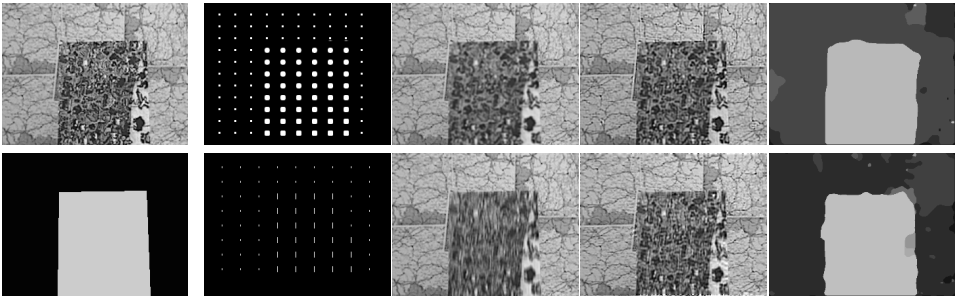

Ground truth Kernel grid Blurred image Restored image Estimated depth

Figure A3: Synthetic Experiment on 'Map' image (Middlebury dataset): The ground truth (GT) latent image and depth map used are shown in first column. The kernel grids generated using the GT depth map for defocus (first row) and motion blur (second row) are shown in the second column. The synthesized blurred image, our deblurring result and estimated depth map are shown, respectively, in the last three columns.

An additional synthetic example is provided in Fig. A3. The ground truth latent image and depth-map taken from the Middlebury dataset are shown in the first column. The latent image is blurred by both defocus and motion blur to produce the blurred inputs shown in column three. Our restored result and depth map are, respectively, shown in the fourth and fifth columns. The comparative results along with PSNR values are shown in Fig. A4. In defocus blur case, though NCSR and SRDB algorithms deblur the foreground layer properly, they introduce heavy artifacts in background layer. In contrast, our method deblurs both the layers effectively and results in better PSNR. Our method outperforms the state-of-the-art qualitatively as well as quantitatively for motion deblurring too.

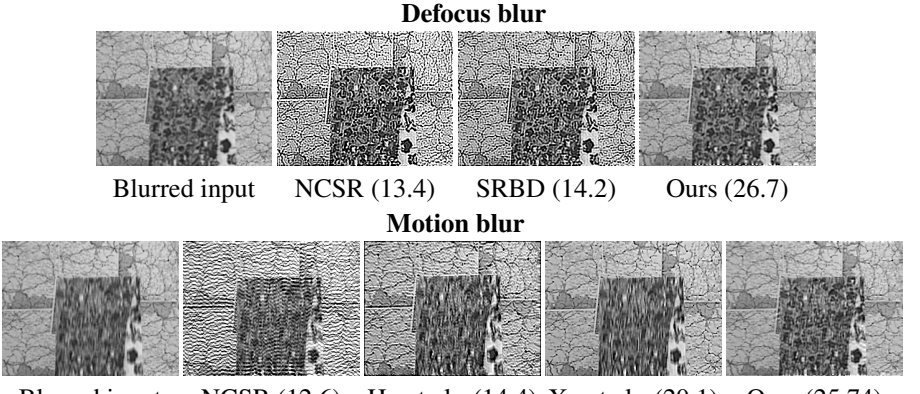

Figure A4: Comparison results for Map dataset. The PSNR values (in dB) are given in bracket.

1.1 Comparison with CDL [26]

There also exists a work on coupled dictionary-based deblurring (CDL) [26]. As this method is quite restrictive, we did not give comparisons with it in the main paper. It considers only Gaussian blur and assumes a priori known number of blur kernels; else it must learn

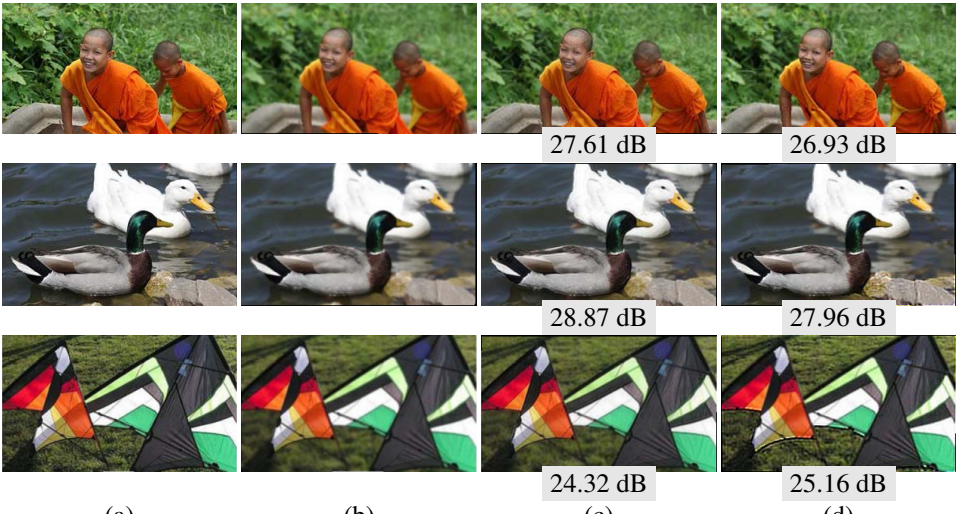

Figure A5: Comparison results with [26]. (a) Latent image. (b) Blurred input. (c) Deblurred result of [26]. (d) Our result. PSNR values are also shown.

a coupled dictionary for each blur kernel making it computationally quite complex. This becomes cumbersome for real 3D scenes since the depth is unknown which necessitates learning dictionaries for many kernels. It does not explicitly calculate any depth map (unlike our method). Since their code is not available online, we ran our method on some of the synthetic examples given in that paper. No real examples are given in [26] for the multi-blur situation. The results provided in [26] are compared with the output of our method in Figs. A5(c) and (d), respectively. Although our method does not perform dictionary learning for each kernel, it performs on par with [26] and even outperforms it in the kite example (third row). Here, the ground is better deblurred by our method.

2 Additional real experiments

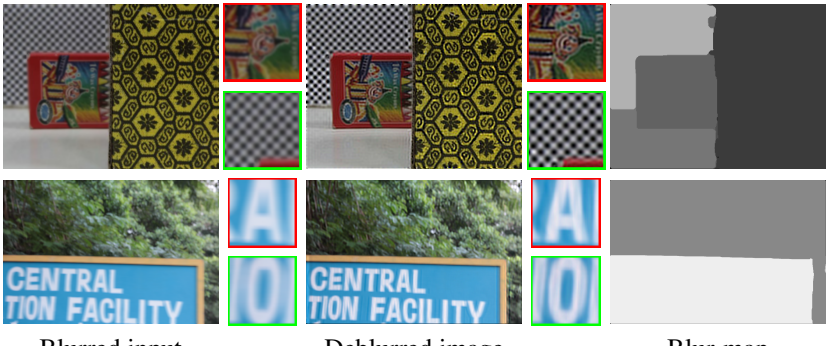

Figure A6: Additional results on defocus and motion blur.

An indoor experiment for the defocus case is shown in Fig. A6 first row. The input is near focused with the box in the front in focus and the defocus effect increasing with depth.

The deblurred result obtained by our method removes the defocus effect at the rear end and produces an all-focused image. The estimated blur-map here corresponds to the relative depth of the scene. The second row of Fig. A6 depicts a real outdoor example for the motion blur scenario. The input image has the sign board in the front which is highly blurred when compared to the background. Here, the blur-depth relation is inverse. The deblurred result and the estimated blur-map are also shown in Fig. A6.